# REPORT No. 253

## FLOW AND DRAG FORMULAS FOR SIMPLE QUADRICS

By A. F. Zahm

### PREFACE

In this text are given the pressure distribution and resistance found by theory and experiment for simple quadrics fixed in an infinite uniform stream of practically incompressible fluid. The experimental values pertain to air and some liquids, especially water; the theoretical refer sometimes to perfect, again to viscid fluids. For the cases treated the concordance of theory and measurement is so close as to make a résumé of results desirable. Incidentally formulas for the velocity at all points of the flow field are given, some being new forms for ready use derived in a previous paper and given in Tables I, III. A summary is given on page 536.

The computations and diagrams were made by Mr. F. A. Louden. The present text is a slightly revised and extended form of Report No. 312, prepared by the writer for the Bureau of Aeronautics in June, 1926, and by it released for publication by the National Advisory Committee for Aeronautics. A list of symbols follows the text.

### PRESSURE AND PRESSURE DRAG

We assume the fluid, of constant density and unaffected by weight or viscosity, to have in all the distant field a uniform velocity $q_0$ parallel to $x$; in the near field the resultant velocity $q$. If now the distant pressure is everywhere $p_0$, and the pressure at any point in the disturbed flow is $p_0 + p$, the superstream pressure $p$ is given by Bernouilli's formula,

$$p/p_n = 1 - q^2/q_0^2, \tag{1}$$

where $p_n = \rho q_0^2/2$, called the "stop" or "stagnation" or "nose" pressure.

At any surface element the superpressure exerts the drag $\int p \, dy \, dz$, whose integral over any zone[1] of the surface is the zonal pressure drag,

$$D = \int p \, dy \, dz. \tag{2}$$

Values of $p$, $D$ are here derived for various solid forms and compared with those found by experiment.

### PRESSURE MEASUREMENTS

The measured pressures here plotted were obtained from some tests by Mr. R. H. Smith and myself in the United States Navy 8-foot wind tunnel at 40 miles an hour. Very accurate models of brass, or faced with brass, had numerous fine perforations, one at the nose, others further aft, which could be joined in pairs to a manometer through fine tubing. Thus the pressure difference between the nose and each after hole could be observed for any wind speed. Then a fine tube with closed tip and static side holes was held along stream at many points abreast of the model, to show the difference of pressure there and at the nose. Next the tube was thrust right through the model, to find the static pressure before and behind it. The method is too well known to require further description.

### THE SPHERE

Assume as the fixed body a sphere, of radius $a$, in a uniform stream of inviscid liquid, as shown in Table I. Then by that table the flow speeds at points on the axis $x$, $y$ and on the surface are

$$q_x = (1 - a^3/x^3)q_0, \qquad q_y = (1 + a^3/2y^3)q_0, \qquad q_t = 1.5q_0 \sin\theta, \tag{3}$$

where $\theta$ is the polar angle. Figure 1 shows plots of these equations.

[1] A zone is a part of the surface bounded by two planes normal to $q_0$. Usually one plane is assumed tangent to the surface at its upstream end.

To graph $p/p_n$ in Figure 1, we subtract from the line $y=1$, first $q_x^2/q_0^2$ to show the pressure along $x$; then $q_t^2/q_0^2$ to portray the surface pressure. A similar procedure gives the superpressure in the equatorial plane.

The little circles show the actual superpressures found with a 2-inch brass sphere in a tunnel wind at 40 miles an hour. These agree well with the computed pressures except where or near where the flow is naturally turbulent.

By (3) and (1), on the sphere's surface $p/p_n = 1-2.25\ \sin^2\theta$; hence the zonal pressure drag $\int p.2\pi y dy$ is

$$D = \pi a^2 \sin^2\theta (1 - \frac{9}{8}\sin^2\theta) p_n, \tag{4}$$

for a nose cap whose polar angle is $\theta$. With increase of $\theta$, as in Figure 2, $D/p_n$ increases to a maximum .698 $a^2$ for $\theta = 41°-50'$ and $p=0$; then decreases to zero for $\theta = 70°-37'$; then to its minimum $-.3927\ a^2$ for $\theta = \pi/2$; then continues aft of the equator symmetrical with its fore part. Thus the drag is decidedly upstream on the front half and equally downstream on the

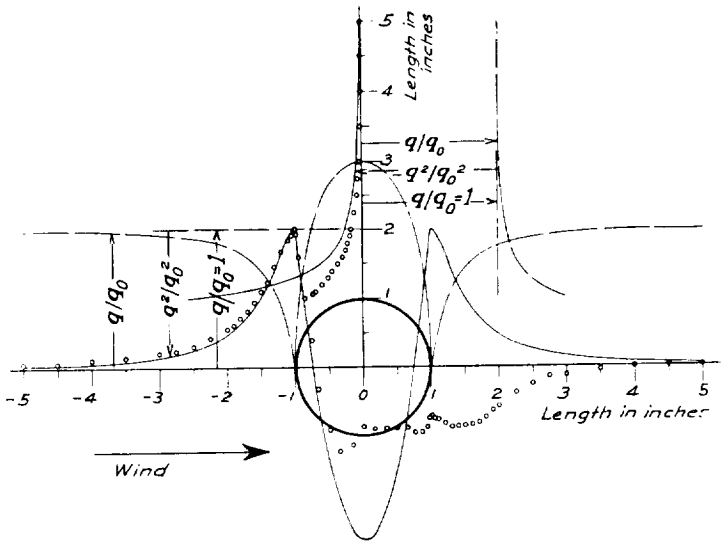


FIG. 1.—Velocity and pressure along axes and over surface of sphere; graphs indicate theoretical values: circles indicate pressures measured at 40 miles per hour in 8-foot wind tunnel, United States Navy

rear half, having zero resultant. The little crosses, giving $D/p_n$ for the measured pressures, show that the total pressure drag in air is downstream, and fairly large for a body so blunt as the sphere.

Figure 3 depicts the whole-drag coefficient [2] $C_D = 2D/\pi\ \rho\ a^2 q_0^2$, of a sphere, for the manifold experimental conditions specified in the diagram, plotted against Reynolds Number $R = 2\ q_0 a/\nu$, $\nu$ being the kinematic viscosity. For $0.2 < R < 200000$, the data lie close to the line.

$$C_D = 28R^{-.85} + .48, \tag{5}$$

an empirical formula devised by the writer as an approximation.

For $.5 < R < 2$ (5) fairly merges with Oseen's formula

$$C_D = 24R^{-1} + 4.5, \tag{6}$$

and for $R < .2$ Stokes' equation $C_D = 24/R$ is exactly verified. Both these formulas are theoretical. Stokes treated only viscous resistance at small scale; Oseen added to Stokes' drag coefficient, $24/R$, the term 4.5 due to inertia.

[2] From the drag $D = C_{D_n} S$, where $S$ is the model's frontal area, one derives the drag coefficient $C_D = D/p_n S$.

Over an important $R$ range Figure 3 shows $C_D = .5$, giving as the sphere's whole drag

$$D = .5\ p_n\ S, \tag{7}$$

where $S = \pi\ a^2$ is the frontal area. That is, the sphere's drag equals half its nose pressure times its frontal area. For $R < .2$ Stokes' value, $D = 6\pi\ \mu\ a\ q_0$, has been exactly verified experimentally, as is well known.

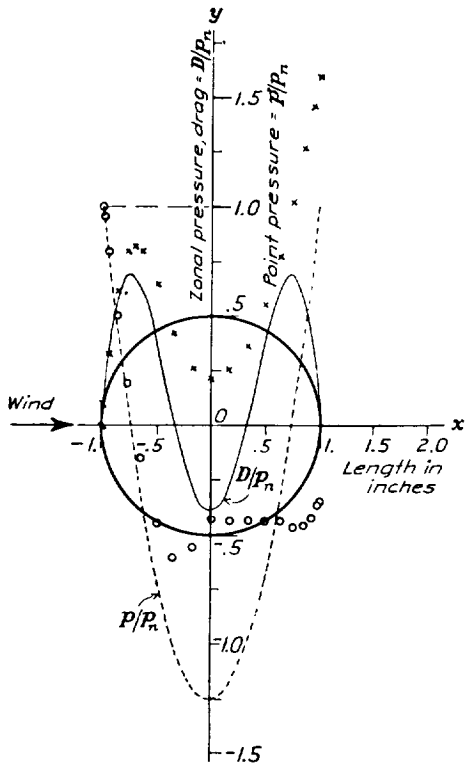


FIG. 2.—Pressure and pressure-drag on sphere. Graphs indicate theoretical values; circles indicate pressure $p/p_n$ measured at 40 miles per hour; crosses indicate pressure-drag $D/p_n$, computed from measured pressure

## THE ROUND CYLINDER

Next assume an endless circular cylinder, of radius $a$, fixed transverse to the stream, as indicated in Table I. By that table the flow speed at points on the axes $x$, $y$ and on the surface is

$$q_x = (1 - a^2/x^2)\ q_0,\ q_y = (1 + a^2/y^2)\ q_0, \qquad q_t = 2\ q_0 \sin\theta, \tag{8}$$

where $\theta$ is the polar angle. Plots of (8) are shown in Figure 4.

Graphs of $p/p_n$, made as explained for the sphere, are also given there, together with experimental values, marked by small circles, for an endless 2-inch cylinder in a tunnel wind at 40 miles an hour. The agreement is good for points well within the smooth-flow region.

On the surface $p/p_n = 1 - 4\ \sin^2\theta$. The integral $2\int_0^y p\,dy$ gives, per unit length of cylinder, the zonal pressure-drag formula,

$$D/p_n = 2\ a \sin\theta - \frac{8}{3}\ a \sin^3\theta. \tag{9}$$

42488—27——34

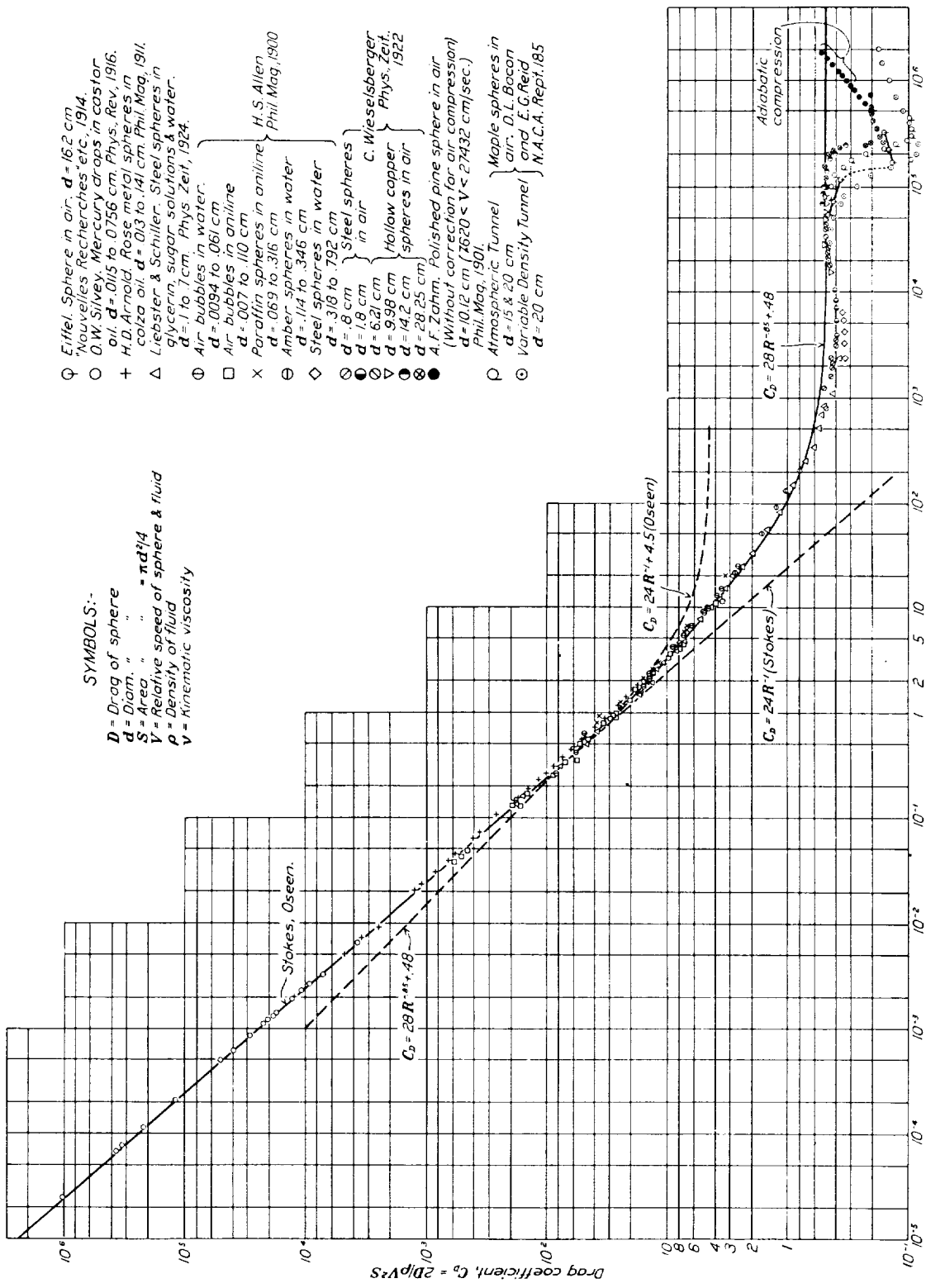


FIG. 3.—Drag coefficient for a sphere in steady translation through a viscous fluid

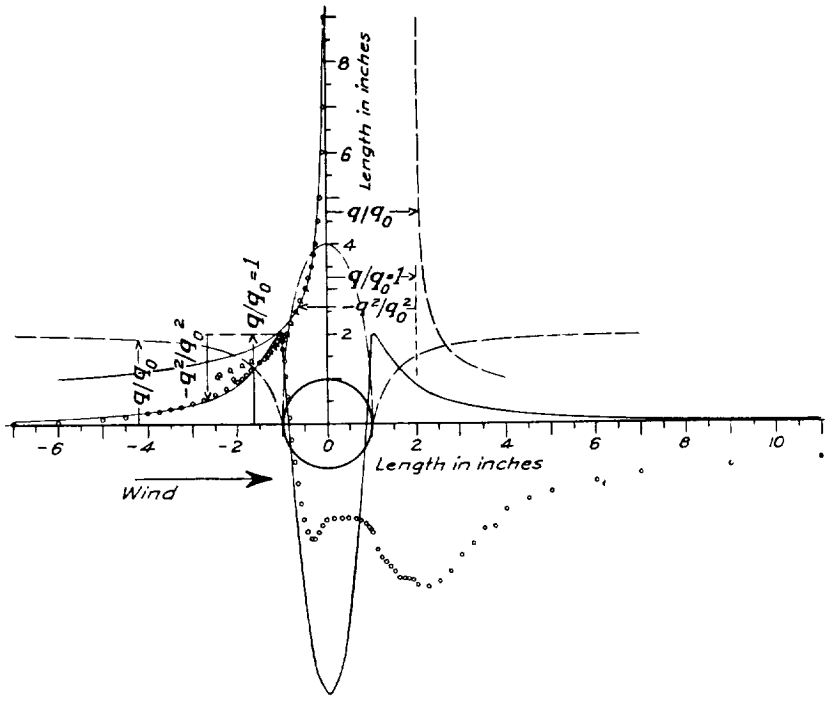


FIG. 4.—Velocity and pressures along axes and over surface of endless cylinder; graphs indicate theoretical values; circles indicate pressures measured at 40 miles per hour in 8-foot wind tunnel, United States Navy

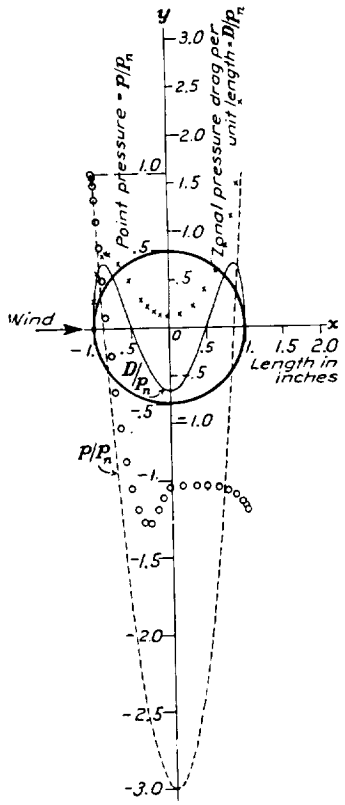


FIG 5.—Pressure and pressure-drag on endless cylinder. Graphs indicate theoretical values; circles indicate pressure $p/p_s$ measured at 40 miles per hour; crosses indicate pressure-drag $D/p_s$ computed from measured pressure

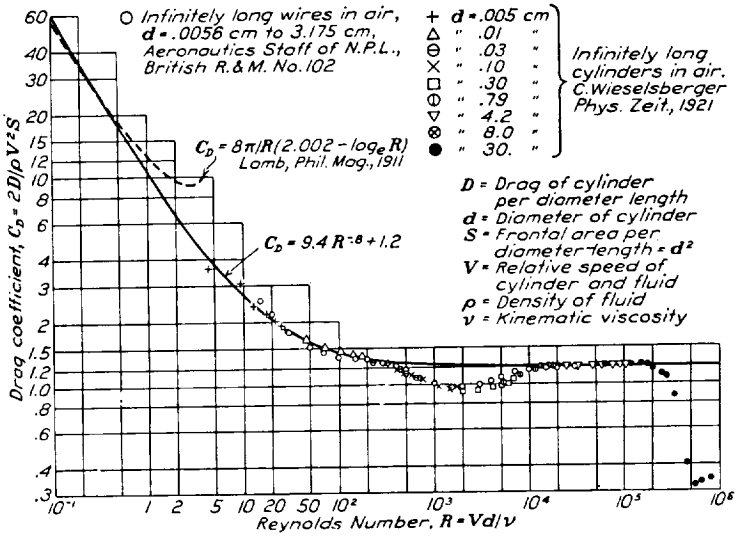


FIG. 6.—Drag coefficient for an endless cylinder in steady translation through a viscous fluid

This is $0, 2a/3$ (max.), $0, -2a/3$, for $\theta = 0°, 30°, 60°, 90°$; and is symmetrical about the equatorial plane $x = 0$. In Figure 5, the little crosses give $D/p_n$ for the measured pressures, and show total $D/p_n = 2.33a$.

Figure 6 delineates the drag coefficient $C_D$ plotted against $R = 2\,aq_0/\nu$, from Wieselsberger's (Reference 1) wind tunnel tests of nine endless cylinders held transverse to the steady flow. The faired line is the graph of

$$C_D = 9.4R^{-.3} + 1.2, \tag{10}$$

an empirical equation devised by the present writer.

For very low values of $R$, Lamb derives the formula

$$C_D = \frac{8}{(2.002 - \log_e R)R}, \tag{11}$$

whose graph in Figure 6 nearly merges with (10) at $R = .3$.

For $15000 < R < 200000$, Figure 6 gives $C_D = 1.2$; hence the drag per unit frontal area is

$$D = 1.2p_n, \tag{12}$$

which is 2.4 times that for the sphere, given by (7).

## THE ELLIPTIC CYLINDER

An endless elliptic cylinder held transverse to the stream, as shown in Table I, gives for points on $x$, $y$ and on its surface,

$$q_x = (1-n)q_0, \qquad q_y = (1+m)q_0, \qquad q_t = (1 + b/a)q_0 \sin\theta, \tag{13}$$

where $m$, $n$ are as in Table I. Amidships $q_t = (1 + b/a)q_0 = 2q_0$ for $a = b$, as given by (8). Graphs of (13) are given in Figure 7.

To find $a'$, $b'$ for plotting (13), assume $a'$ and with it as radius strike about the focus an arc cutting $y$. The cutting point is distant $b'$ from the origin. Otherwise, $b' = \sqrt{a'^2 - c^2}$, where $c^2 = a^2 - b^2 = \text{const.}$

With $a/b = 4$ one plots $p/p_n$ in Figure 7, as explained for the sphere. The circles give the experimental $p/p_n$ for an endless 2-inch by 8-inch strut, at zero pitch and yaw, in a tunnel wind at 40 miles an hour. The theoretical and measured pressures agree nicely for all points before, abreast, and well behind the cylinder.

Again, $\sin^2\theta = a^2y^2/(b^4 + c^2y^2)$, if $c^2 = a^2 - b^2$. Hence on the model

$$p/p_n = 1 - q_t^2/q_0^2 = 1 - \frac{(a+b)^2y^2}{b^4 + c^2y^2}. \tag{14}$$

This gives the zonal pressure drag, $D = 2\int_0^y p\,dy$, per unit length of cylinder, or

$$D/p_n = 2y - 2(a+b)^2 \int_0^y \frac{y^2\,dy}{b^4 + c^2y^2} = -4b\,\frac{a+b}{c^2}\,y + 2b^2\,\frac{(a+b)^2}{c^3}\tan^{-1}\frac{cy}{b^2}. \tag{15}$$

whose graph, for $a/b=4$, appears in Figure 8. It rises from 0 at the nose to its maximum where $p=0$, then falls to its minimum amidships.

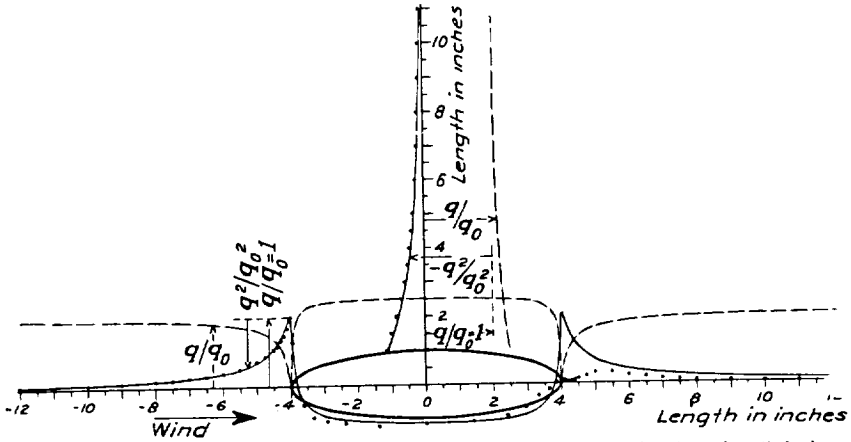


FIG. 7.—Velocity and pressure along axes and over surface of endless elliptic cylinder. Graphs indicate theoretical values; circles indicate pressure measured at 40 miles per hour in 8-foot wind tunnel, United States Navy

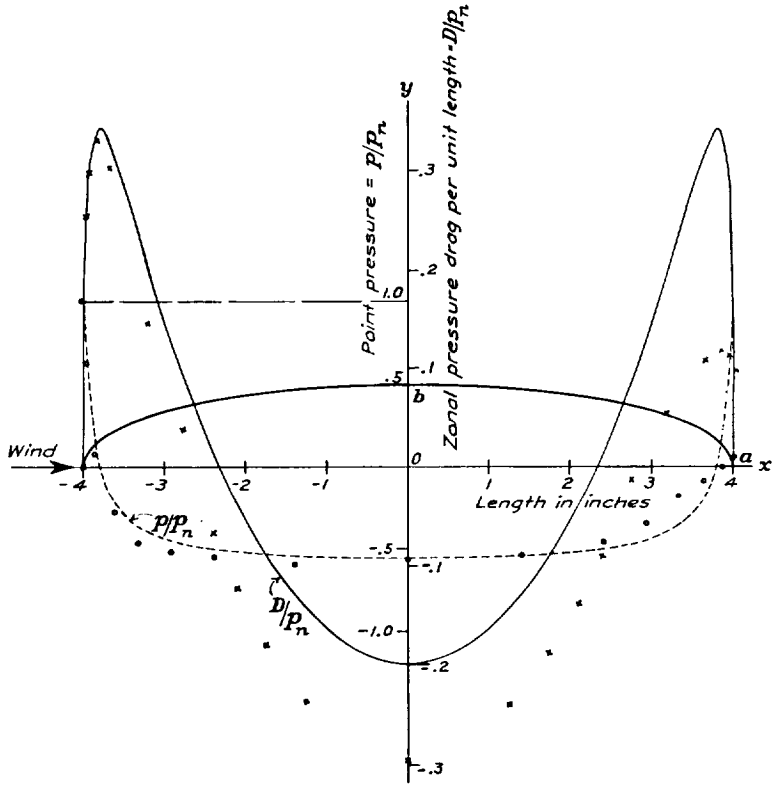


FIG. 8.—Pressure and pressure-drag on endless elliptic cylinder. Graphs indicate theoretical values; circles indicate pressure $p/p_n$ measured at 40 miles per hour; crosses indicate pressure-drag $D/p_n$ computed from measured pressure

Whatever the value of $a/b$, the whole pressure on the front half is negative or upstream, as for the sphere and round cylinder, and is balanced by the rear drag. For $b$ fixed it decreases indefinitely with $b/a$.

The crosses marking actual values of $D/p_n$ found in said test show a downstream resultant $D$. In fact, it is one-third the whole measured drag of pressure plus friction, or one-half the friction drag.

For the cylinder held broadside on, $b>a$ and $a^2-b^2=-c^2$, hence changing $c^2$ to $-c^2$ under the integral sign of (15), we find

$$D/p_n=-4b\frac{a+b}{c^2}y-b^2\frac{(a+b)^2}{c^3}\log_e\frac{b^2+cy}{b^2-cy}, \tag{16}$$

where now $c^2=b^2-a^2$. With $b$ fixed, the upstream pressure drag on the front half increases with $b/a$, becoming infinite for a thin flat plate. It is balanced by a symmetrical drag back of the plate.

Such infinite forces imply infinite pressure change at the edges where, as is well known, the velocity can be $q=\sqrt{2p_r/p}=\infty$, in a perfect liquid whose reservoir pressure is $p_r=\infty$. Otherwise viewed, the pressure is $p_r$ at the plate's center (front and back) and decreases indefinitely toward the edges, thus exerting an infinite upstream push on the back and a symmetrical downstream push on the front. In natural fluids no such condition can exist.

## THE PROLATE SPHEROID

A prolate spheroid, fixed as in Table I, gives for points on $x$, $y$ and the solid surface, respectively, the flow speeds

$$q_x=(1-n)q_0, \qquad q_y=(1+m)q_0, \qquad q_t=(1+k_a)\,q_0\sin\theta, \tag{16}$$

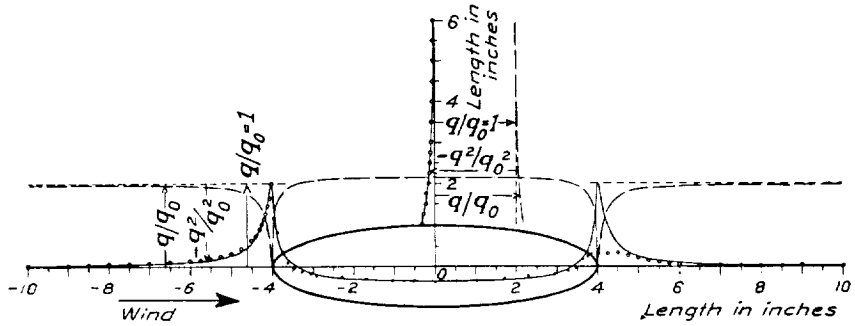


FIG. 9.—Velocity and pressure along axes and over surface of prolate spheroid. Graphs indicate theoretical values; circles indicate pressures measured at 40 miles per hour in 8-foot wind tunnel, United States Navy; dots give pressures found with an equal model in British test, R. and M. No. 600, British Advisory Committee for Aeronautics

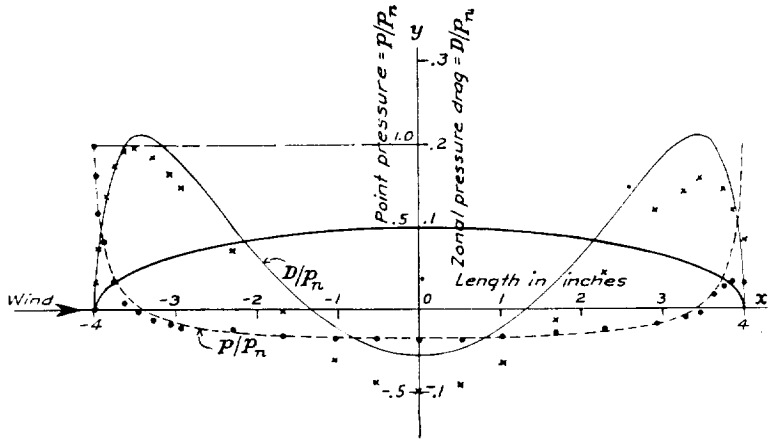


FIG. 10.—Pressure and pressure-drag on prolate spheroid. Graphs indicate theoretical values; dots indicate measured pressure $p/p_n$ from Figure 9; crosses indicate pressure-drag $D/p_n$ computed from measured pressure

where $k_a$ is to be taken from Table II. Graphs of (16) are given in Figure 9, for a model having $a/b=4$, viz., $k_a=0.082$.

For this surface $p/p_n$ plots as in Figure 10. For a 2 by 8 inch brass model values of $p/p_n$ are shown by circles for a test at 40 miles an hour in the United States Navy tunnel; by dots for a like test in a British tunnel. (Reference 2.)

By (16), for points on the surface $p/p_n=1-q_t^2/q_0^2=1-(1+k_a)^2\sin^2\theta$. From this, since $\sin^2\theta=a^2y^2/(b^4+c^2y^2)$, the zonal pressure drag $\int p.\,2\pi y\,dy$ is found. Thus

$$D/p_n=\pi y^2-\frac{\pi a^2}{c^2}(1+k_a)^2y^2+\frac{\pi a^2b^4}{c^4}(1+k_a)^2\log.\frac{b^4+c^2y^2}{b^4}. \tag{17}$$

Starting from $y=0$, $D/p_n$ increases to its maximum when $p=0$, or $\sin\theta=1/(1+k_a)$; then diminishes to its minimum for $y=b$. Figure 10 gives the theoretical and empirical graphs of $D/p_n$ for $a/b=4$.

For $b$ fixed the upstream drag on the front half decreases indefinitely with $b/a$, becoming zero for infinite elongation.

## OBLATE SPHEROID

The flow velocity about an oblate spheroid with its polar axis along stream is given by formulas in Table I, and plotted in Figure 11, together with computed values of $p/p_n$. No determinations of $p$ or $D$ were made for an actual flow. The formula for $D/p_n$ is like (17), except that $c^2=b^2-a^2$, and $k_a$ is larger for the oblate spheroid, as seen in Table II. For $b$ fixed the upstream drag on the front half increases indefinitely with $b/a$.

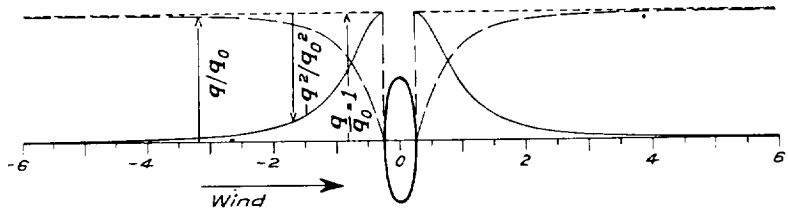


FIG. 11.—Theoretical velocity and pressure along x axis of oblate spheroid. Diameter/thickness = 4

## CIRCULAR DISK

The theoretical flow speeds and superpressures for points on the axis of a circular disk fixed normal to a uniform stream of inviscid liquid are plotted in Figure 12, without comparative data from a test. One notes that the formulas are those for an oblate spheroid with eccentricity $e=1$.

For $1500<q_0\,a/\nu<500000$, Wieselsberger (Reference 3) finds for the air drag of a thin normal disk, of area $S$,

$$D=1.1\,p_nS, \tag{18}$$

or 2.2 times that for a sphere. For $aq_0/\nu$ extremely small, theory gives

$$D=5.1\,\pi\,\mu\,a\,q_0, \tag{19}$$

as is well known. Test data for a complete graph, including these extremes, are not yet available.

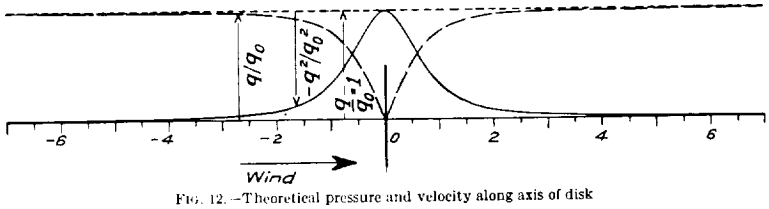


FIG. 12.—Theoretical pressure and velocity along axis of disk

## REGIONS OF EQUAL SPEED

In the flow field $q$, $p$ are constant where $q_t^2 + q_n^2 = \text{constant}$, viz. where

$$q^2/q_0^2 = (1+m)^2 \sin^2\theta + (1-n)^2 \cos^2\theta = \text{const.} \tag{20}$$

In particular for the region $q = q_0$, this becomes

$$\tan^2\theta = \frac{n}{m}\frac{2-n}{2+m} = \frac{a'^4}{b'^4}\tan^2\beta^* \tag{21}$$

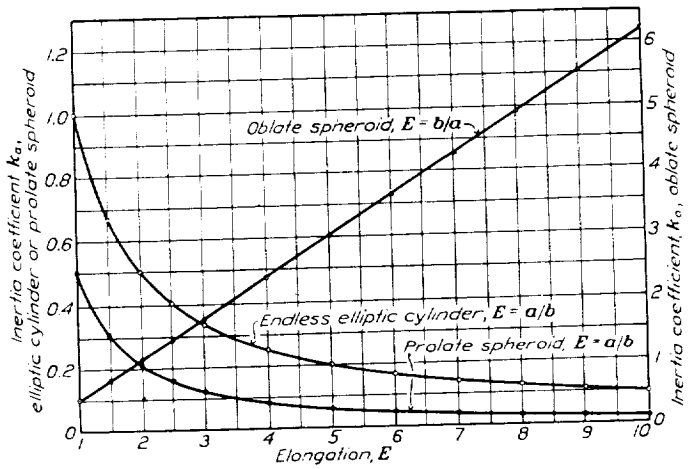


FIG. 13.—Inertia coefficient vs. elongation. Plotted from Table II

which applies to all the quadrics in Table I. Clearly tan $\theta = 0$ for $n = 2$; $\tan^2\theta = n/m$ for $m$, $n = 0$, viz. for all distant points of (21). For these points the normal to any confocal ellipse lies along the radius vector and asymptote of (21), as seen in Figures 14 to 17.

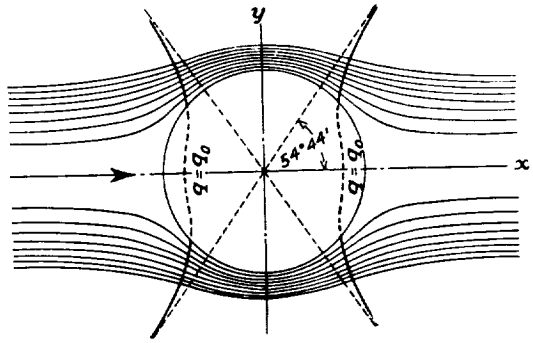


FIG. 14.—Lines of steady flow, lines of constant speed and pressure, for infinite frictionless liquid streaming past a sphere

For the sphere $n = 2m = a^3/r^3$; hence (21) becomes

$$\tan^2\theta = 2\frac{2r^3 - a^3}{2r^3 - .5a^3} \tag{22}$$

where $r = a' = \sqrt{x^2 + y^2}$. The form of this is depicted in Figure 14.

* $\tan\beta = y/x$ is the slope of a radial line through the point $(x, y)$ where (21) cuts a confocal curve $a'b'$, of Table I. Knowing $a'$, $b'$, $\beta$, to locate $(x, y)$ draw across the radial line an arc of $a'b'$ by sliding along the $x$, $y$ axes a straightedge subdivided as in the ellipsograph. The operation is rapid and easy.

For a round cylinder $n = m = a^2/r^2$; hence

$$\tan^2\theta = \frac{2r^2 - a^2}{2r^2 + a^2} \text{ or, } 2r^2 = a^2 \sec 2\theta, \tag{23}$$

which is the section of a hyperbolic cylinder, as in Figure 15.

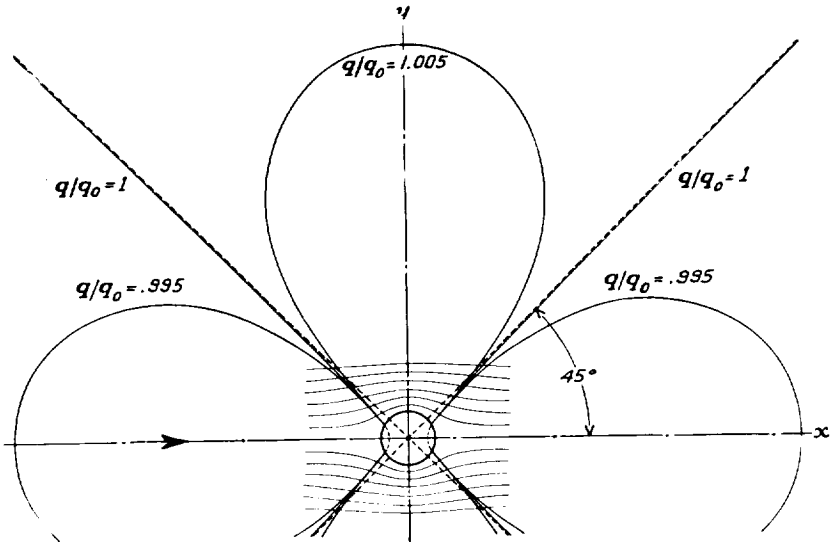


FIG. 15.—Lines of steady flow, lines of constant speed and pressure, for infinite frictionless liquid streaming across endless round cylinder

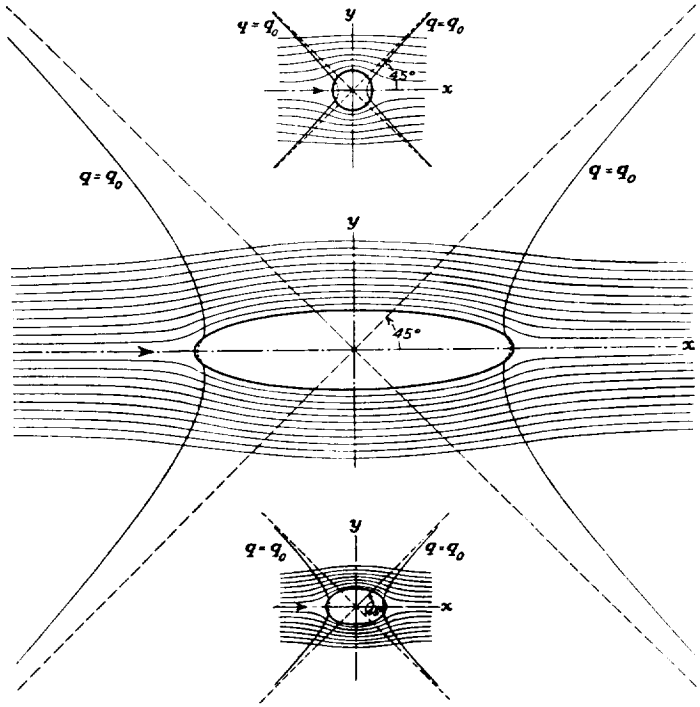


FIG. 16.—Lines of steady flow, lines of constant speed and pressure, for infinite frictionless liquid streaming across endless elliptic cylinder

A plot of (21) for an elliptic cylinder, fixed as shown in Table I, is given in Figure 16; for a prolate spheroid in Figure 17.

Besides the region (21), having $q = q_o$, it is useful to know the limit of perceptible disturbance say where $q^2/q_o^2 = 1 \pm .01$. This in (20) gives

$$(1+m)^2 \sin^2\theta + (1-n)^2 \cos^2\theta = 1 \pm .01, \tag{24}$$

which applies to all the quadrics here studied. Hence

$$\tan^2\theta = \frac{n}{m}\,\frac{2-n}{2+m} \pm \frac{0.01}{m(2+m)\cos^2\theta}, \tag{25}$$

A graph of (25) for a round cylinder is shown in Figure 15. Like plots for the other quadrics

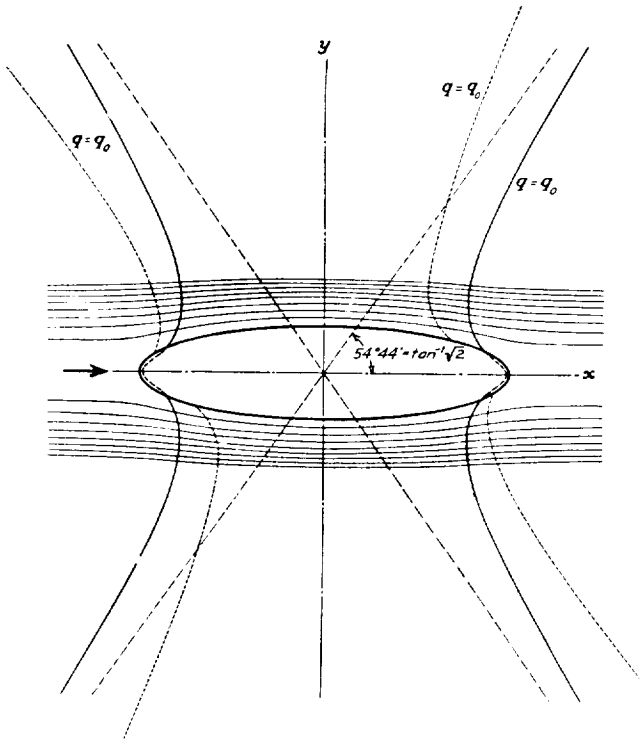


FIG. 17.—Lines of steady flow, lines of constant speed and pressure, for infinite frictionless liquid streaming past a prolate spheroid. Full-line curve $q = q_o$ refers to stream parallel to $x$; dotted curve $q = q_o$ refers to stream inclined 10° to $x$

If in (20) a series of constants be written for the right member, the graphs compose a family of lines of equal velocity and pressure, covering the entire flow field. Rotating Figures 14, 17 about $x$ gives surfaces of $q = q_o$.

## COMPARISON OF SPEEDS

Before all the fixed models the flow speed is $q_o$ at a great distance and 0 at the nose; abreast of them it is $q_o$ at a distance, and $(1+k_a)q_o$ amidships.

The flux of $q - q_o$ through the equatorial plane obviously must equal $q_o S$ where $S$ is the body's frontal area. Hence two bodies having equal equators have the same flux $q_o S$, and the same average superspeed or average $q - q_o$. But the longer one has the lesser midship speed;

## SYMBOLS USED IN TEXT

| | |
|---|---|
| $x$, $y$ | Cartesian coordinates; also axes of same. |
| $r$, $\beta$ | Polar coordinates. |
| $\alpha$ | Angle of attack of uniform stream. |
| $s$ | Length of arc, increasing with $\beta$. |
| $\theta$ | Inclination to $x$ of normal to confocal curves in Table I. |
| $\varphi$ | Velocity function. |
| $\psi$ | Stream function. |
| $q$ | Resultant velocity at any point of fluid. |
| $q_o$ | Velocity of distant fluid (parallel to $x$ axis). |
| $q_x$, $q_y$ | Velocity at points on $x$ and $y$ axes (parallel to $x$ axis). |
| $q_t$ | Velocity along confocal surface or model surface. |
| $q_n$ | Velocity normal to confocal surface. |
| $\rho$ | Density of fluid. |
| $\mu$ | Viscosity. |
| $\nu$ | Kinematic viscosity. |
| $p_n$ | Nose pressure $=\rho q_o^2/2$. |
| $p_o$ | Pressure in distant fluid. |
| $p$ | Superstream pressure anywhere. |
| $D$ | Zonal pressure drag $=\int p\,dy\,dz$. |
| $D$ | Whole drag. |
| $S$ | Frontal area of model. |
| $C_D$ | Drag coefficient $=D/p_nS$. |
| $R$ | Reynolds number. |
| $a$ | Radius of sphere, cylinder. |
| $a$, $b$ | Semiaxes of ellipse. |
| $a'$, $b'$ | Semiaxes of confocal ellipse. |
| $e$ | Eccentricity of ellipse. |
| $e'$ | Eccentricity of confocal ellipse. |
| $c$ | Focal distance $=ae=a'e'=\sqrt{a^2-b^2}$ |
| $k_a$ | Inertia factor (Table II). |
| $m$, $n$, $m_s$ | Quantities defined in Tables I, II. |
| $\epsilon$ | Colatitude (see equation 30). |

## TABLE I

Flow functions for simple quadrics fixed in a uniform stream of speed $q_o$ along $x$ positive

| Symbol definitions | Form of quadric | Value of functions at any confocal surfaces of semiaxes $a'$, $b'$: Velocity function $\varphi$ | Stream function $\psi$ | Component velocities $q_t$, $q_n$ |
|---|---|---|---|---|
| See diagram A (fig. 20) | Sphere | $\varphi=-(1+m)\,q_o x$, where $m=\frac{a^3}{2a'^3}$ | $\psi=-\frac{1}{2}(1-n)\,q_o y^2$, where $n=\frac{a^3}{a'^3}$ | Differentiation along arc $s$ of either figure gives: $q_t=\frac{\partial\varphi}{\partial x}\frac{dx}{ds}=(1+m)\,q_o \sin\theta$, valid for all the figures; $q_n=\frac{\partial\psi}{\partial y}\frac{dy}{ds}=-(1-n)\,q_o \cos\theta$, for the cylinders; $q_n=\frac{1}{y}\frac{\partial\psi}{\partial y}\frac{dy}{ds}=-(1-n)\,q_0\cos\theta$, for the axial surfaces; viz., sphere, spheroids, disk. For $a'$, $b'=a$, $b$, Table II gives $m_s$; whence $q_t=(1+m_s)\,q_o\sin\theta$, as the flow velocity on a fixed quadric surface. $q_n=\pm 0$ for disk, since $n=1$ *Remark*—both $q_t$, $q_n$ can be derived from either $\varphi$ or $\psi'$. If $q_t$, $q_n=$ max. $q_t$, $q_n$ on $a'b'$, at any other point thereof $q_t=q_t\sin\theta$, $q_n=q_n\cos\theta$ |
| | Circular cylinder | $\varphi=-(1+m)\,q_o x$, $m=\frac{a^2}{a'^2}$ | $\psi=-(1-n)\,q_o y$, $n=\frac{a^2}{a'^2}$ | |
| See diagram B (fig. 20) | Elliptic cylinder | $\varphi=-(1+m)\,q_o x$, $m=\frac{b}{a'}\frac{a+b}{a'+b'}$ | $\psi=-(1-n)\,q_o y$, $n=\frac{b}{b'}\frac{a+b}{a'+b'}$ | |
| | Prolate spheroid $e=\frac{1}{a}\sqrt{a^2-b^2}$ | $\varphi=-(1+m)\,q_o x$, $m=-\frac{\log_e\frac{1+e'}{1-e'}-2e'}{\log_e\frac{1+e}{1-e}-2e}$ | $\psi=-\frac{1}{2}(1-n)\,q_o y^2$, $n=\frac{\log_e\frac{1+e'}{1-e'}-\frac{2e'}{1-e'^2}}{\log_e\frac{1+e}{1-e}-\frac{2e^2}{1-e^2}}$ | |
| See diagram C (fig. 20) | Oblate spheroid $e=\frac{1}{b}\sqrt{b^2-a^2}$ | $\varphi=-(1+m)\,q_o x$, $m=-\frac{\frac{e'b'}{a'}-\sin^{-1}e'}{\frac{ea}{b}-\sin^{-1}e}$ | $\psi=-\frac{1}{2}(1-n)\,q_o y^2$, $n=\frac{\frac{e'a'}{b'}-\sin^{-1}e'}{\frac{ea}{b}-\sin^{-1}e}$ | |
| | Circular disk $a=0$, $e=1$ | $\varphi=-(1+m)\,q_o x$, $m=\frac{2}{\pi}\left(\frac{b'}{a'}-\sin^{-1}e'\right)$ | $\psi=-\frac{1}{2}(1-n)\,q_o y^2$, $n=-\frac{2}{\pi}\left(\frac{a'b}{b'^2}-\sin^{-1}e'\right)$ | |

$\varphi$, $\psi$, in elliptic coordinates, can be found in textbooks; e. g., §§ 71,105,108, Lamb's Hydrodynamics, 4th Ed.

hence its outboard speed wanes less rapidly with distance along $y$. A like relation obtains along $x$ from the nose forward. These relations are shown in the velocity graphs of Figures 18 and 19. A figure similar to 18, including many models, is given in Reference 4.

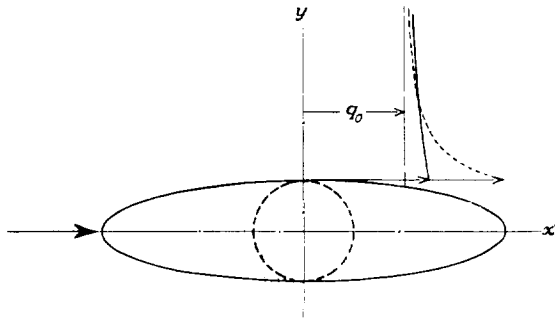


FIG. 18.—Superposed graphs of flow speed abreast of endless round and elliptic cylinders of same thickness fixed transverse to an infinite stream of inviscid liquid. At great distance flow speed is $q_0$.

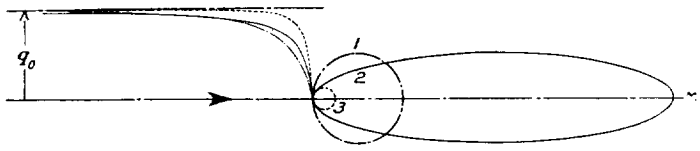


FIG. 19.—Superposed graphs of axial flow speed before three endless cylinders 1, 2, and 3 (3 osculating 2), each fixed transverse to an infinite stream of inviscid liquid. At great distance flow speed is $q_0$.

## COMPARISON OF PRESSURES

The foregoing speed relations determine those of the pressures. The nose pressures all are $p_n = \rho q_o^2/2$; the midship ones are $p = p_n - (1+k_a)^2 p_n$. The drag on the front half of the model is upstream for all the quadrics here treated; it increases with the flatness, as one proves by (15), (17), and is infinite for the normal disk and rectangle.

## APPLICATION OF FORMULAS

The ready equations here given, aside from their academic interest in predicting natural phenomena from pure theory, are found useful in the design of air and water craft. The formula for nose pressure long has been used. That for pressure on a prolate spheroid, of form suitable for an airship bow, is so trustworthy as to obviate the need for pressure-distribution measurements on such shapes. The same may be said of the fore part of well-formed torpedoes deeply submerged. The computations for stiffening the fore part of airship hulls can be safely based on theoretical estimates of the local pressures. The velocity change, well away from the model, especially forward of the equatorial plane, can be found more accurately by theory than by experiment. The equation (21) of undisturbed speed shows where to place anemometers to indicate, with least correction, the relative speed of model and general stream.

## REFERENCES

1. WIESELSBERGER, C.: Physicalische Zeitschrift, vol. 22. 1921.
2. JONES, R., and WILLIAMS, D. H.: The distribution of pressure over the surface of airship model U. 721, together with a comparison with the pressure over a spheroid. Brit. Adv. Com. for Aeron. Reports and Memoranda No. 600. 1919.
3. WIESELSBERGER, C.: Physicalische Zeitschrift, vol. 23. 1922.
4. TAYLOR, D. W.: Speed and Power of Ships, gives a figure similar to 18 but including more models. 1910.

TABLE II

Inertia factors $k_a$* for quadric surfaces in steady translation along axis $a$ in Figure 20

| Elongation $E$ | Elliptic cylinder, $E=a/b$ $k_a=\frac{b}{a}$ | Prolate spheroid $E=a/b$ $k_a=-\frac{\log_e \frac{1+e}{1-e}-2e}{\log_e \frac{1+e}{1-e}-\frac{2e}{1-e^2}}$ | Oblate spheroid $E=b/a$ $k_a=-\frac{eE^2-E\sin^{-1}e}{e-E\sin^{-1}e}$ |
|---|---|---|---|
| 1.00 | 1.000 | 0.500 | 0.500 |
| 1.50 | .667 | .305 | .803 |
| 2.00 | .500 | .209 | 1.118 |
| 2.50 | .400 | .157 | 1.428 |
| 3.00 | .333 | .121 | 1.742 |
| 4.00 | .250 | .082 | 2.379 |
| 5.00 | .200 | .059 | 3.000 |
| 6.00 | .167 | .045 | 3.642 |
| 7.00 | .143 | .036 | 4.279 |
| 8.00 | .125 | .029 | 4.915 |
| 9.00 | .111 | .024 | 5.549 |
| 10.00 | .100 | .021 | 6.183 |
| $\infty$ | .000 | .000 | $\infty$ |

* In this table $k_a=m_a$ of Table I, viz. the value of $m$ when $a', b'=a, b$. Lamb (R. and M. No. 623, Brit. Adv. Com. Aeron.) gives the numerical values in the third column above. For motion of elliptic cylinder along $b$ axis inertia factor is $k_b=a/b$.

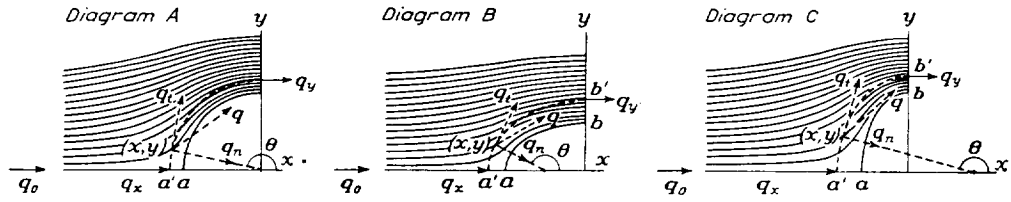


FIG. 20

## VELOCITY AND PRESSURE IN OBLIQUE FLOW [2]

### PRINCIPLE OF VELOCITY COMPOSITION

A stream $q_0$ oblique to a model can be resolved in chosen directions into component streams each having its individual velocity at any flow point, as in Figure 21. Combining the individuals gives their resultant, whence $p$ is found.

### VELOCITY FUNCTION

Let a uniform infinite stream $q_0$ of inviscid liquid flowing past a fixed ellipsoid centered at the origin have components $U$, $V$, $W$ along $x$, $y$, $z$, taken parallel, respectively, to the semi-axes, $a$, $b$, $c$; then we find the velocity potential $\varphi$ for $q_0$ as the sum of the potentials $\varphi_a$, $\varphi_b$, $\varphi_c$ for $U$, $V$, $W$.

In the present notation textbooks prove, for any point $(x, y, z)$ on the confocal ellipsoid $a'\ b'\ c'$,

$$\varphi_a=-(1+m_a)Ux, \tag{26}$$

and give as constant for that surface

$$m_a=abc\left(1-abc\int_a^\infty \frac{da'}{a'^2\,b'\,c'}\right)^{-1}\int_\lambda^\infty \frac{da'}{a'^2\,b'\,c'}\ * \tag{27}$$

the multiplier of $\int_\lambda^\infty$ being constant for the model, and $\lambda=a'^2-a^2$. Adding to (26) analogous values of $\varphi_b$, $\varphi_c$ gives

$$\varphi=-(1+m_a)Ux-(1+m_b)Vy-(1+m_c)Wz\equiv-(1+m)q_0h, \tag{28}$$

[2] This brief treatment of oblique flow was added by request after the preceding text was finished.

* Simple formulas for this integral and the corresponding $b$, $c$ ones, published by Greene, R. S. Ed. 1833, are given by Doctor Tuckerman in Report No. 210 of the National Advisory Committee for Aeronautics for 1925. Some ready values are listed in Tables III, IV.

where $h$ is the distance of $(x, y, z)$ from the plane $\varphi = 0$, and $m_a$, $m_b$, $m_c$, $m$ are generalized inertia coefficients of $a'\ b'\ c'$ for the respective streams $U$, $V$, $W$, $q_0$. For the model itself the inertia coefficients usually are written $k_a$, $k_b$, $k_c$, $k$. The direction cosines of $h$ are

$$L = \frac{1+m_a}{1+m}\frac{U}{q_0},\quad M = \frac{1+m_b}{1+m}\frac{V}{q_0},\quad N = \frac{1+m_c}{1+m}\frac{W}{q_0}, \tag{29}$$

as appears on dividing (28) by $(1+m)q_0$, the resultant of $(1+m_a)U$, $(1+m_b)V$, $(1+m_c)W$.

### EQUIPOTENTIALS AND STREAMLINES

On $a'\ b'\ c'$ the plane sections $\varphi = \text{constant}$ are equipotential ellipses parallel to the major section $\varphi = O$, and dwindling fore and aft to mere points, which we call stream poles, where the plane (28) is tangent to $a'\ b'\ c'$. If $\epsilon$ is the angle between any normal to $a'\ b'\ c'$ and the polar

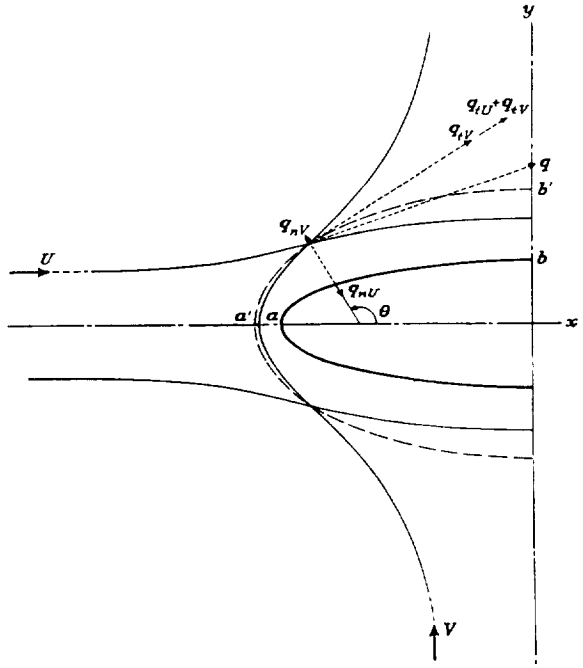


FIG. 21.—Superposition of streamline velocities for component plane flows parallel to axes of elliptic cylinder

normal, whose direction cosines are $L$, $M$, $N$, we call the line $\epsilon = \text{const.}$ a line of stream latitude. Thus $\epsilon$ is the colatitude or obliquity of a surface element of $a'\ b'\ c'$. The line $\epsilon = 90°$ is the stream equator. This latter marks the contact of a tangent cylinder parallel to the polar normal, viz, perpendicular to the plane (28), as in Figure 22. If $l$, $m$, $n$ are the direction cosines of any normal to $a'\ b'\ c'$

$$\cos\epsilon = lL + mM + nN. \tag{30}$$

Since the streamlines all cut the equipotentials squarely,[3] the polar streamline must run continuously normal to the family of confocal ellipsoids $a'\ b'\ c'$. Hence it forms the intersection of a pair of confocal hyperboloids, and at infinity asymptotes a line parallel to $q_0$ through the origin. This straight line may be called the stream axis. Its equation is $x : y : z = U : V : W$.

[3] On the model, therefore, the streamlines are longitude lines, viz. orthogonals to the latitude lines.

### COMPONENT VELOCITIES

At any point of any confocal surface $a'\ b'\ c'$ the streamline velocity $q$, perpendicular to the equipotential ellipse there, has components $q_n$, $q_t$, respectively, along the surface normal $n$ and the tangent $s$ in the plane of $q$ and $n$. By (28) we have

$$q_t = \frac{\partial \varphi}{\partial h}\frac{dh}{ds} = \bar{q}_t \sin \epsilon, \tag{31}$$

where $-\partial\varphi/\partial h = (1+m)q_0 \equiv q_t = \text{max. } q_t$, is the equatorial velocity. By (26) the inward normal velocity due to $\varphi_a$ is

$$-\frac{\partial}{\partial_n}(1+m_a)Ux = -l(1-n_a)U, \tag{32}$$

$n_a$ being constant on $a'\ b'\ c'$, as may be shown. Similarly, $\varphi_b$, $\varphi_c$ contribute $-m(1-n_b)V, -n(1-n_c)W$; hence the whole normal component is

$$q_n = -l(1-n_a)U - m(1-n_b)V - n(1-n_c)W = q_n \cos \epsilon, \tag{33}$$

where $\bar{q}_n = [(1-n_a)^2U^2 + (1-n_b)^2V^2 + (1-n_c)^2W^2]^{.5} = \text{max. } q_n$ is the normal velocity at the stream poles. Some values of $n_a$, $n_b$ are given in Tables I, III. One also may find (33) as the normal derivative of (28).

We now state (28): At any point of $a'\ b'\ c'$ the velocity potential equals $\bar{q}_t h$, the equatorial speed times the distance from the plane of zero potential. Similarly (31) (33) state: At any point of $a'\ b'\ c'$ the tangential speed ($\bar{q}_t \sin \epsilon$) equals the equatorial speed times the sine of the obliquity; the normal speed ($q_n \cos \epsilon$) equals the polar speed times the cosine of the obliquity. This theorem applies to all the confocals, even at the model where $q_n = 0$.[4]

Incidentally the normal flux through $a'\ b'\ c'$ is $\int \bar{q}_n \cos \epsilon \cdot dS = \bar{q}_n \int dS_\phi$, where $S_\phi$ is the projection of $S$ on the plane of $\phi = \text{const.}$ and equals the cross section of the tangent cylinder. The whole flux through $a'\ b'\ c'$ is therefore zero, as should be.

### POLAR STREAMLINE

Some of the foregoing relations are portrayed in Figure 22 for a case of plane flow. Noteworthy is the polar streamline or hyperbola. Starting at infinity parallel to $q_0$, the polar filament runs with waning speed normally through the front poles of the successive confocal surfaces; abuts on the model at its front pole, or stop point; spreads round to the rear pole; then accelerates downstream symmetric with its upstream part. Its equation $q_t = 0 = \partial\phi/\partial s$ can be written from (28)

$$q_t = (1+m_a)U \sin \theta - (1+m_b)V \cos \theta = 0, \text{ or } \tan \theta = \frac{1+m_b}{1+m_a}\frac{V^*}{U} \tag{34}$$

This asymptotes the stream axis $y/x = V/U$; for at infinity $m_a$, $m_b = 0$, and $\tan \theta = V/U$. Plane-flow values of $m_a$, $m_b$ are given in Tables I, III.

All the confocal poles are given by (34); those of the model are at the stops where

$$\tan \theta = \frac{1+k_a}{1+k_b}\frac{V}{U} = \frac{a^2}{b^2}\frac{y}{x}. \tag{37}$$

Thus on an elliptic cylinder they are where $y/x = b^3/a^3 \cdot V/U$; on a thin lamina they are at $x = \pm c \cos \alpha$, as given in the footnote. Tables II, IV give values of $k_a$, $k_b$.

---

[4] An analogous theorem obtains also for any other uniform steady stream, say of heat or electricity, that has zero normal component at the boundary ellipsoid and zero concentration in the flow field.

[5] To graph (34) we may use the known relations.

$$\tan \theta = \frac{a'^2}{b'^2}\frac{y}{x} = \frac{a'}{b'}\tan \alpha, \tag{35}$$

where $\tan \alpha = V/U$ is the slope of $q_0$ or the asymptote to (34). Thus (34) becomes $a'/b' = (1+m_b)/(1+m_a)$, which with the tabulated values of $m_a$, $m_b$, reduces to

$$\frac{x^2}{c^2 \cos^2 \alpha} - \frac{y^2}{c^2 \sin^2 \alpha} = 1, \tag{36}$$

a hyperbola whose semiaxes are $c \cos \alpha$, $c \sin \alpha$, $c$ being the focal distance. In this treatment $x = a' \cos \alpha$, $y = b' \sin \alpha$, $\alpha$ being a fixed eccentric angle of the successive confocal elipses.

Each angle of attack has its own flow pattern; each its polar streamline given by (34). A close-graded family of confocal ellipses and hyperbolas therefore portrays all the poles and polar streamlines in the plane $ab$ for all angles of attack. The family can be written

$$x = a' \cos \alpha, \qquad y = b' \sin \alpha. \tag{38}$$

Thus, giving $a'$, $b'$ a set of fixed values, then $\alpha$ a set, we have the confocal families

$$\frac{x^2}{a'^2} + \frac{y^2}{b'^2} = 1. \qquad \frac{x^2}{c^2 \cos^2 \alpha} - \frac{y^2}{c^2 \sin^2 \alpha} = 1. \tag{39}$$

the first being ellipses, the second hyperbolas like (36) below.

Similarly, the locus $q_n = 0$, or $q = q_t$, is written from (33). With $W = 0$,

$$\tan \theta = -\frac{1 - n_a}{1 - n_b} \frac{U}{V}. \tag{40}$$

Its discussion is of minor interest.

### DRAG AND MOMENT

Formulas for the pressure $p$ all over the simple quadrics here treated are well known, for oblique as well as axial flow, and serve to find the drag and moment. For uniform flow the resultant drag is zero; its zonal parts can be found as heretofore. The moment about $z$ is the surface integral of $p(y\, dy\, dz - x\, dx\, dz)$, and generally is not zero.

### REGIONS OF EQUAL SPEED ABOUT OBLIQUE MODELS

Compounding the velocities (31), (33) at any point in the $ab$ plane, as in Figure 22, gives for $q$ constant

$$q^2 = [(1 + m_a) U \sin \theta - (1 + m_b) V \cos \theta]^2 + [(1 - n_a) U \cos \theta + (1 - n_b) V \sin \theta]^2 = \text{const.} \tag{41}$$

In particular for $q^2 = U^2 + V^2$ (41) gives

$$\tan \theta = \frac{K}{B} (A \pm \sqrt{BC + A^2}) = \frac{a'^2}{b'^2} \tan \beta. \tag{42}$$

where $K = V/U$, and

$$A = (1 + m_a)(1 + m_b) - (1 - n_a)(1 - n_b), B = m_a(2 + m_a) - n_b(2 - n_b) K^2, C_D = \frac{n_a(2 - n_a)}{K^2} - m_b(2 + m_b).$$

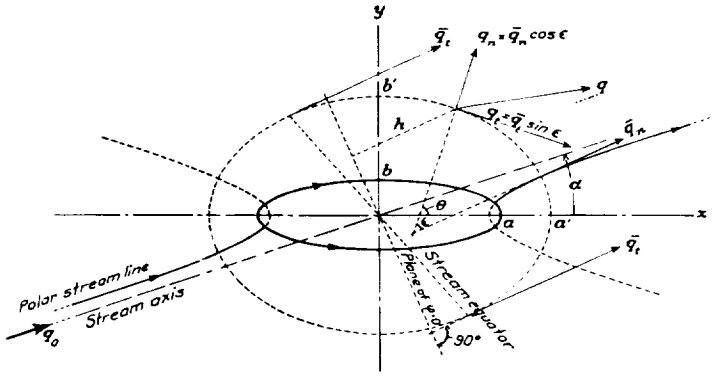


FIG. 22.—Polar streamline and component velocities for uniform stream of inviscid liquid about oblique elliptic cylinder

For an elliptic cylinder, as is well known.

$$m_a = \frac{b}{a'} \frac{a + b}{a' + b'}, \qquad n_a = \frac{b}{b'} \frac{a + b}{a' + b'}, \qquad m_b = \frac{a}{b'} \frac{a + b}{a' + b'}, \qquad n_b = \frac{a}{a'} \frac{a + b}{a' + b'},$$

which determines $A$, $B$, $C$, and thence $\beta$ in terms of $a'$ $b'$. Thus, for an endless elliptic cylinder of semiaxes $a = 4$, $b = 1$, yawed 10° to the stream, i. e., $V/U = \tan 10° = .1763$, the graph of (42) has the form shown full line in Figure 23. This graph takes the dotted form when $V = 0$, $q_0 = U$.

For a prolate spheriod of semiaxes $a=4$, $b=1$, yawed 10°, the graph of (42) is shown in Figure 17.

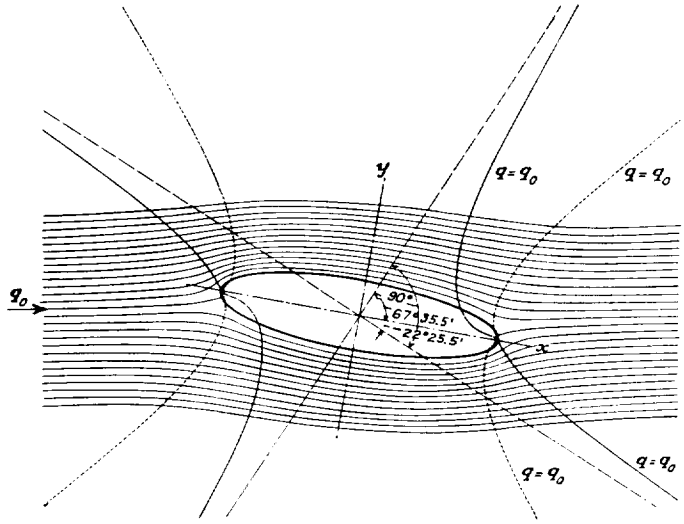


FIG. 23.—Lines of steady flow, lines of constant speed and pressure, for infinite frictionless liquid streaming across endless elliptic cylinder. Dotted curve refers to stream parallel to $x$; full-line curve $q=q_o$ refers to stream inclined 10° to $x$

The two values of tan $\beta$ in (42) are

$$\tan\beta_1=\frac{K}{B}(A+\sqrt{BC+A^2}),\qquad \tan\beta_2=\frac{K}{B}(A-\sqrt{BC+A^2}),\tag{43}$$

from which are readily derived

$$\tan(\beta_1-\beta_2)=\frac{2K\sqrt{BC+A^2}}{B-K^2C},\qquad \tan(\beta_1+\beta_2)=\frac{2KA}{B+K^2}.\tag{44}$$

(43) give the $x$-ward inclinations $\beta_1$, $\beta_2$, of the asymptotes of the curves $q=q_o$. As can be proved, the interasymptote angle $\beta_1-\beta_2$ remains constant as $K(=V/U)$ varies and the asymptotes rotate through $\frac{1}{2}(\beta_1+\beta_2)$ about the $c$ axis.

Thus, with an elliptic cylinder, giving $A$, $B$, $C$ their values at $\infty$ makes

$$\tan(\beta_1-\beta_2)=\infty,\qquad \tan(\beta_1+\beta_2)=\frac{K(a+b)}{b-aK^2};\tag{45}$$

hence the asymptotes continue rectangular, as in Figure 23, while with varying angle of attack they rotate through $\frac{1}{2}(\beta_1+\beta_2)$. Or more generally one may show that $\frac{d}{da}(\beta_1-\beta_2)=0\therefore\beta_1-\beta_2=$ const.

A similar treatment applies to the other figures of Table III. For all the cylinders the interasymptote angle is 90°; for the spheroids it is $2\tan^{-1}\sqrt{2}=109°-28'$ in the $ab$ plane. Figure 17 is an example. If the flow past the spheroids is parallel to the $bc$ plane the interasymptote angle for the curves $q=q_o$ in that plane is obviously unaffected by stream direction. It is 90° for infinitely elongated spheroids; $109°-28'$ for all others. Excluded from the generalizations of this paragraph are the infinitely thin figures, such as disks and rectangles edgewise to the stream, that cause no disturbance of the flow. Passing to three dimensions, we note that the asymptotic lines form asymptotic cones having their vertex at the origin.

42488—27——35

**SUMMARY**

For an infinite inviscid liquid streaming uniformly, in any direction, past an ellipsoid or simple quadric:

1. The velocity potential at any confocal surface point equals the greatest tangential speed along that surface times the distance from the point to the surface's zero-potential plane.

2. The tangential flow speed at said surface point equals the greatest tangential speed times the sine of the obliquity, or inclination of the local surface element to the equipotential plane.

3. The normal speed at the point equals the greatest normal speed times the cosine of the obliquity.

4. The locus of $q=q_o$ is a cup-shaped surface asymptoting a double cone with vertex at the center.

5. The vertex angle of this cone is invariant with stream direction; for cylinders it is 90°, for spheroids it is $2\tan^{-1}\sqrt{2}=109°-28'$.

6. The velocity and pressure distribution are closely the same as for air of the same density, except in or near the region of disturbed flow.

7. The zonal drag is upstream on the fore half; downstream on the rear half; zero on the whole. These zones may be bounded by the isobars, $\epsilon$ const.

For the same stream, but with kinematic viscosity $\nu$, if the dynamic scale is $R=q_od/\nu$, $d$ being the model's diameter:

8. The drag coefficient of a sphere is $24/R$ for $R<.2$; $28R^{-.85}+.48$ for $0.2<R<200{,}000$; and 0.5 for $10^4<R<10^5$.

9. The drag coefficient of an endless round cylinder fixed across stream is $8\pi/R(2.002-\log_eR)$ for $R<.5$; approximately $9.4\ R^{-.8}+1.2$ for $0.5<R<200{,}000$; 1.2 for $10^4<R<200{,}000$.

10. For $15{,}000<R<200{,}000$ the drag coefficient of a round cylinder is 2.4 times that for a sphere.

## TABLE III

Flow functions for simple quadrics in stream $V$ along $y$ positive

(For all shapes $\phi = -(1+m_b)\ Vy$, $\quad q_t = (1+m_b)\ V \sin \epsilon^*$ $\quad q_n = -(1-n_b)\ V \cos \epsilon$)

| Shape | $m_b$ | $n_b$ |
|---|---|---|
| Sphere | $\frac{a^3}{2a'^3}$ | $\frac{a^3}{a'^3}$ |
| Circular cylinder | $\frac{a^2}{a'^2}$ | $\frac{a^2}{a'^2}$ |
| Elliptic cylinder | $\frac{a}{b'}\ \frac{a+b}{a'+b'}$ | $\frac{a}{a'}\ \frac{a+b}{a'+b'}$ |
| Prolate spheroid $e=\frac{1}{a}\sqrt{a^2-b^2}$ | $\frac{\log_e \frac{1+e'}{1-e'} - \frac{2e'}{1-e'^2}}{\log_e \frac{1+e}{1-e} - 2e\frac{1-2e^2}{1-e^2}}$ | $\frac{\log_e \frac{1+e'}{1-e'} - 2e'\frac{1-2e'^2}{1-e'^2}}{\log_e \frac{1+e}{1-e} - 2e\frac{1-2e^2}{1-e^2}}$ |
| Oblate spheroid $e=\frac{1}{b}\sqrt{b^2-a^2}$ | $\frac{-e'\sqrt{1-e'^2} - \sin^{-1}e'}{e\frac{1+e^2}{\sqrt{1-e^2}} - \sin^{-1}e}$ | $\frac{e'\frac{1+e'^2}{\sqrt{1-e'^2}} - \sin^{-1}e'}{e\frac{1+e^2}{\sqrt{1-e^2}} - \sin^{-1}e}$ |

* $\epsilon$ is the angle between $b'$ and any normal to the confocal surface.

## TABLE IV

Inertia factors $k_b$ for quadric surfaces in steady translation along axis $b$ in Figure 20

| Elongation $E$ | Ellip. cyl $E=a/b$ $k_b=\frac{a}{b}$ | Prol. spher. $E=a/b$ $k_b=-\frac{\log_e \frac{1+e}{1-e} - \frac{2e}{1-e^2}}{\log_e \frac{1+e}{1-e} - 2e\frac{1-2e^2}{1-e^2}}$ | Obl. spher. $E=b/a$ $k_b=-\frac{e-E\sin^{-1}e}{eE^2(e^2+1)-E\sin^{-1}e}$ |
|---|---|---|---|
| 1.00 | 1.00 | 0.500 | 0.500 |
| 1.50 | 1.50 | .621 | .384 |
| 2.00 | 2.00 | .702 | .310 |
| 2.50 | 2.50 | .763 | .260 |
| 3.00 | 3.00 | .803 | .223 |
| 4.00 | 4.00 | .860 | .174 |
| 5.00 | 5.00 | .895 | .140 |
| 6.00 | 6.00 | .918 | .121 |
| 7.00 | 7.00 | .933 | .105 |
| 8.00 | 8.00 | .945 | .092 |
| 9.00 | 9.00 | .954 | .084 |
| 10.00 | 10.00 | .960 | .075 |
| $\infty$ | $\infty$ | 1.000 | 0 |

The numerical values in column 3 are given in Lamb's paper already cited; those in column 4 are given substantially by Doctor Bateman, Report No. 163 National Advisory Committee for Aeronautics, 1923.